Physical Self-Calibration of X-ray and SZ Surveys

Greg L. Bryan, Zoltan Haiman (Columbia University) and Joshua D. Younger (CfA)

1. Cluster Surveys and Self-Calibration

Clusters of galaxies form at the highest peaks in the primordial density field, and as a result, their abundance and spatial distribution are very sensitive to the underlying cosmology. Several recent works have focused on various aspects of extracting cosmological parameters from high–yield future surveys, such as the statistical constraints available on curvature Ω_k (Holder, Haiman, & Mohr 2001), assessing the impact of sample variance (Hu & Kravtsov 2003) and other uncertainties (Levine, Schultz, & White 2002) on parameter estimates, and controlling such uncertainties by utilizing information from the shape of the cluster mass function dN/dM (Hu 2003).

Most importantly, recent work has focused on the systematic errors on cosmological parameters arising from the inherent uncertainties on the mass–observable relation. It has been shown that large forthcoming cluster surveys can be "self–calibrating", in the sense that when the abundance and clustering properties of clusters are considered in tandem, tight constraints can be derived on cosmology even if the mass–observable relation has to be determined simultaneously from the same data (Majumdar & Mohr 2004; Wang et al. 2004; Lima & Hu 2005). In these studies, the mass–observable relation was assumed to be either unknown a priori, or to have a simple parametric form (such as a power–law).

Recent work on the XMM-LSS survey (Garcet et al. 2007; Pierre et al. 2007; Pacaud et al. 2007) has provided a demonstration of how such a survey could work, but has also pointed out the difficulty of making careful cosmological constraints with self-calibration. In particular, the complications of the unknown-scatter in the mass-observable relations, the complicated mass-flux relation (due to the redshifting of emission lines), the selection function, and Malmquist bias all conspire to reduce the efficiency and accuracy of the simplest self-calibration approach.

While the most simple self-calibration approach may yield interesting constraints with large samples, one may argue that this approach is overly conservative. In particular, it is reasonable to expect that the structure of clusters, such as their mean density and temperature profiles, can be at least approximately computed from ab–initio models. The simplest, spherically symmetric, self–similar models contradict observations, such as the relation between X–ray flux (L_x) and temperature (T), or the resolved profiles of low–mass clusters (Voit et al. 2002). However, motivated by the observations of Ponman et al. (1999), modified–entropy models of the intra–cluster medium (ICM), while still not correct in detail (Pratt & Arnaud 2005; Younger & Bryan 2007), have been successful at predicting the mass–observable scalings in temperature, luminosity, and SZ effect, from first principles (Voit et al. 2002). It is reasonable to expect that our understanding of the physics determining the structure of clusters will be improved in the future by advances in both observations and numerical simulations.

In this contribution, we examine the utility of a partial understanding of the ICM in improving cosmological constraints. We will show that using a–priori cluster structure models, it is possible to significantly improve cosmological constraints, relative to direct, phenomenological self–calibration of the mass–observable relation – even if the physical model has free parameters. Furthermore, the combination of X-ray and SZ datasets is particularly promising (Verde, Haiman, & Spergel 2002), and can more effectively break degeneracies, since the underlying models directly relate the SZ decrement to the X–ray flux. The end result is significantly improved errors on the cosmology, using the same observational data set, in addition to a well constrained model of the ICM.

2. Physical Models of Cluster Structure

Our model is described in detail in Younger et al. (2006), but we summarize it briefly here. Assuming spherical symmetry and hydrostatic equilibrium, together with physically motivated boundary conditions, allows us to calculate the pressure and temperature profiles, which, combined with the gas density, give the entropy distribution as a function of radius. This entropy distribution is then modified by adding a constant K_0 at all radii, and the hydrostatic equilibrium equations are re–integrated under the assumption that mass shells do not cross (i.e. $K(M_g)$ is conserved where M_g is the total gas mass at that radius). The resulting modified density and temperature profiles can be used to predict cluster observables, such as the X–ray flux or SZ decrement. For the fiducial cosmology, we adopt $(\Omega_m h^2, \Omega_{DE}, w_0, w_a, \sigma_8, \Omega_b h^2, n_s) = (0.14, 0.73, -1.0, 0, 0.7, 0.024, 1.0)$.

Our aim is to quantify the merits of using a model for the cluster, as opposed to directly self–calibrating the mass–observable relation, as proposed in previous studies (Majumdar & Mohr 2004; Wang et al. 2004) which parametrized the X–ray luminosity and SZ flux as power-laws.

3. Simulating Galaxy Cluster Surveys

Our mock X–ray survey has a flux detection threshold of $F_x(0.5-2.0 \text{ keV}) = 3 \times 10^{-14}$ erg cm^2 s^{-1}. In our fiducial model, this yields a cluster surface density of ~ 5.5 deg^{-2}. The mock SZ survey is modeled after upcoming observations by the South Pole Telescope (Ruhl et al. 2004; Wang et al. 2004), with a limiting SZ flux of $S_\nu = 3.0$ mJy at $\nu = 150$ GHz. This flux threshold produces a yield that again matches the cluster counts of 5.5 deg^{-2} in the mock X–ray survey, allowing an easy comparison. The fiducial power-law parameters are chosen to match the local scalings.

In both surveys, and for both the physical and phenomenological model, we consider the case of 20 flux bins with a log–normal scatter that has a fiducial value of $\sigma_{\log M|\Psi} = 0.1$ for both the X–ray and SZ mass-observable relation (Lima & Hu 2005), but is assumed to be a free parameter. For each of these, we consider two different descriptions of the entropy injection history. First, we fit a power-law evolution of the entropy floor of the form $K_0(z) = K_0(z=0)(1+z)^{\alpha_K}$, with K_0 and α_K as free parameters. Second, we consider arbitrary evolution of the entropy floor K_0, in which K_0 is fit independently in each of 40 redshift bins of width $\Delta z = 0.05$. In both of these cases, the fiducial entropy floor is set to $K_0 = 125 h^{1/3}$ keV cm^2 with no evolution. Finally, for the purpose of comparison, the sky coverage in both surveys is taken to be $\Delta\Omega = 4000$ deg^2, the size planned for SPT (Ruhl et al. 2004). For surveys covering a different solid angle, the constraints we obtain below scale as $\propto \Delta\Omega^{-1/2}$.

The constraints are presented in Table 1 and Figure 1. In this table, we show the Fisher matrix constraints for each parameter as well as a synergy coefficient ζ_δ, to quantify the fractional improvement in the marginalized error on a parameter p_δ after combining experiments versus adding the individual experiment errors in quadrature (Younger et al. 2006). The synergy coefficient ranges from 1 for no improvement from combining the experiments beyond adding the individual constraints in quadrature, to 0 if the degeneracies are fully broken, in the limiting case that the combined Fisher matrix delivers a perfect knowledge of p_δ.

In looking at this table, we see some gain in combining X-ray and SZ surveys for the phenomenological model,. However, the physical model gives smaller degeneracy coefficients and better absolute constraints for all parameters. In particular, using the physical model improves w_0 and w_a constraints by a factor of 2 relative to the phenomenological model. We also note that allowing arbitrary K_0–evolution still does not significantly degrade constraints, even in the presence of uncertain scatter, relative to a power–law K_0–evolution. Interestingly, we find that this is because for a physical model with arbitrary K_0 evolution, the

X–ray and SZ surveys are exceptionally complementary. In particular, the synergy coefficient for the dark energy parameters $\zeta_{w_0,w_a} < 0.7$, indicating that constraints improve by more than 30% (over adding the constraints in quadrature) when the X–ray and SZ surveys are combined. This is illustrated visually in Figure 1, where we show marginalized constraints in the $w_0 - w_a$ plane. The figure shows a significant reduction in the size of the error ellipse when the two surveys are combined. In particular, this reduction is much more significant in the physical model (left panel) than in the case of the phenomenological model (right panel).

Though these results above are promising, we here note some important reservations. Firstly, the goal in our study is to motivate a methodology, rather than a specific cluster structure model. We believe that the improvement in the constraints in individual experiments arises because adopting a physical model introduces new cosmology sensitivity that is not present when the mass–observable relation is parametrized directly. For the preheated model we consider here, the dominant effect is the new $\Omega_m h^2$–sensitivity, which we expect to hold generically, regardless of the details of a cluster model. Likewise, the improvement in the synergy between the SZ and X–ray surveys arises because the physical model relates the X–ray flux and the SZ decrement (one cannot be changed without changing the other). This, again, should be a generic feature of any model that directly models the ICM gas distribution.

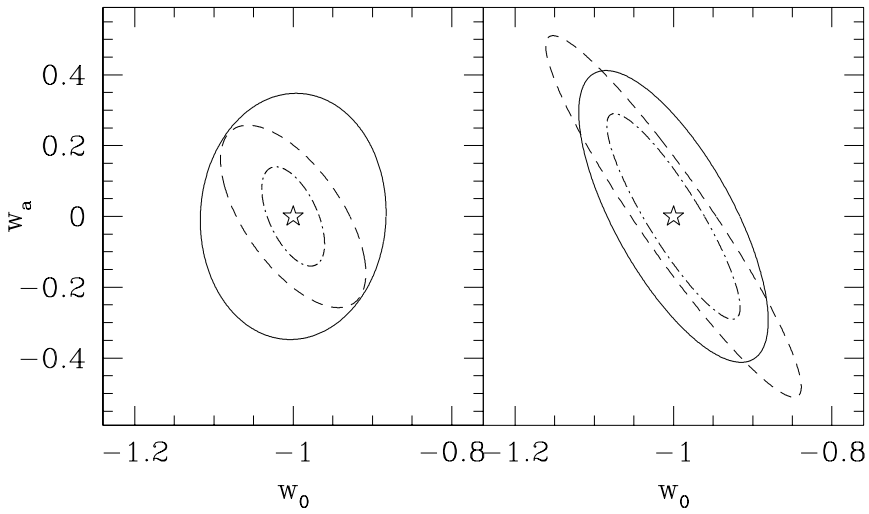

Fig. 1.— Parameter constraints in the $w_0 - w_a$ plane for direct self–calibration of the mass–observable relation (right panel) and using the physical model (left panel). The constraints have been marginalized over all other cosmological parameters. The figure assumes $n_{bin} = 20$ independent flux bins, and a log–normal scatter in the mass–observable relation that is aprori unknown (with the fiducial value of $\sigma_{\log M|\Psi} = 0.1$; see Table 1). In both panels, we show constraints from the mock X–ray (solid ellipses) and SZ (dashed ellipses) surveys individually, and from the combination of the two surveys (dot–dashed ellipses). Note the improved degeneracy breaking in the physical model, when data from the two surveys are combined.

4. Conclusions

Using a Fisher Matrix approach, we have demonstrated that the use of a physically motivated model of the ICM in mock large-scale cluster surveys gives significantly better constraints on cosmological and model parameters, and better synergy between SZ and X–ray surveys, than one can obtain by directly parametrizing the mass–observable relation. In particular, when both the cosmology and model parameters are included in the fit, for the simplest case of pure cluster counts as a function of redshift, the physical model yields constraints on the dark energy equation of state that are 2 times tighter and 3 times less degenerate in the X–ray, and 10 times tighter and 15 times less degenerate in the SZ than those using a phenomenological model. If the shape of the mass function and scatter in the mass-observable relation are included and the entropy floor is taken to be an arbitrary function of redshift (see Table 1), the dark energy parameter constraints are 20% times tighter and 2 times less degenerate in the X–ray, and 2 times tighter and 2 times less degenerate in the SZ than those using a phenomenological model. In addition, these constraints are up to a factor of two tighter than those from simply adding the individual experiment errors in quadrature, relative to a minor 20% improvement from combining constraints using a phenomenological model. These result suggest that parametrized physical models of cluster structure will be useful when extracting constraints on both cosmology, and cluster structure itself, from future large–scale SZ and X–ray cluster surveys.

REFERENCES

Arnaud, M. & Evrard, A. E., 1999, MNRAS, 305, 631
Garcet, O., et al. 2007, A&A, 474, 473
Holder, G. P., Haiman, Z., & Mohr, J. J., 2001, ApJ, 560, L111
Hu, W. & Kravtsov, A. V., 2003, ApJ, 584, 702
Hu, W., 2003, Phys. Rev. D, 67, 081304
Lima, M. & Hu, W., 2005, Phys. Rev. D., 72, 043006
Levine, E. S., Schultz, A. E., & White, M., 2002, ApJ, 577, 569
Lloyd-Davies, E. J., Ponman, T. J., & Cannon, D. B., 2000, MNRAS, 315, 689
Majumdar, S. & Mohr, J. J., 2004, ApJ, 613, 41
Pacaud, F., et al. 2007, MNRAS, 382, 1289
Pierre, M., et al. 2007, MNRAS, 382, 279
Ponman, T. J., Cannon, D. B., & Navarro, J. F., 1999, Nature, 397, 135
Pratt, G. W. & Arnaud, M., 2005, A&A, 429, 791
Ruhl, J., et al., 2004, Proc. SPIE, 5498, 11
Verde, L., Haiman, Z., & Spergel, D., 2002, ApJ, 581, 5
Voit, M. G, Bryan, G. L., Balogh, M. L., & Bower, R. G., 2002, ApJ, 576, 601
Wang, S., Khoury, J., Haiman, Z., & May, M., 2004, Phys. Rev. D., 70, 7013008
Younger, J. D., Haiman, Z., Bryan, G. L., & Wang, S. 2006, ApJ, 653, 27
Younger, J. D., & Bryan, G. L. 2007, ApJ, 666, 647

This preprint was prepared with the AAS LaTeX macros v5.2.

Table 1: Self-Calibrated Cluster Constraints for $n_{bin} = 20$ and $\sigma_{\log M|\Psi} = 0.1$ log-Normal scatter.

		$\Delta p(XR)$	$\Delta p(SZ)$	$\Delta p(XR+SZ)$	$\zeta(XR+SZ)$
Phenomenological	$\Delta\Omega_m h^2$	5.93×10^{-3}	2.89×10^{-2}	2.58×10^{-3}	0.44
	$\Delta\Omega_{DE}$	1.43×10^{-2}	1.32×10^{-2}	5.66×10^{-3}	0.58
	Δw_0	7.88×10^{-2}	0.11	5.55×10^{-2}	0.88
	Δw_a	0.27	0.34	0.19	0.91
	$\Delta\sigma_8$	1.40×10^{-2}	1.56×10^{-2}	8.85×10^{-3}	0.85
	$\Delta \log A_x$	2.56×10^{-2}	$\cdots$	1.72×10^{-2}	$\cdots$
	$\Delta\beta_x$	2.09×10^{-2}	$\cdots$	1.22×10^{-2}	$\cdots$
	$\Delta\gamma_x$	9.67×10^{-2}	$\cdots$	5.80×10^{-2}	$\cdots$
	$\Delta\sigma_{XR}$	1.24×10^{-3}	$\cdots$	1.23×10^{-3}	$\cdots$
	$\Delta \log A_{sz}$	$\cdots$	3.20×10^{-2}	2.12×10^{-2}	$\cdots$
	$\Delta\beta_{sz}$	$\cdots$	4.77×10^{-2}	1.36×10^{-2}	$\cdots$
	$\Delta\gamma_{sz}$	$\cdots$	3.32×10^{-2}	2.80×10^{-2}	$\cdots$
	$\Delta\sigma_{SZ}$	$\cdots$	6.25×10^{-3}	5.71×10^{-3}	$\cdots$
Physical Model	$\Delta\Omega_m h^2$	1.66×10^{-3}	1.55×10^{-3}	1.05×10^{-3}	0.92
$K_0(z) = K_0(1+z)^{\alpha_K}$	$\Delta\Omega_{DE}$	2.86×10^{-3}	4.11×10^{-3}	2.22×10^{-3}	0.95
	Δw_0	5.18×10^{-2}	3.03×10^{-2}	2.16×10^{-2}	0.83
	Δw_a	0.13	9.60×10^{-2}	7.30×10^{-2}	0.95
	$\Delta\sigma_8$	9.40×10^{-3}	5.31×10^{-3}	3.33×10^{-3}	0.72
	$\Delta\sigma_{XR}$	6.47×10^{-3}	$\cdots$	4.89×10^{-3}	$\cdots$
	$\Delta\sigma_{SZ}$	$\cdots$	7.55×10^{-3}	6.30×10^{-3}	$\cdots$
	Δf_g	2.09×10^{-2}	2.67×10^{-2}	1.10×10^{-2}	$\cdots$
	ΔK_0	5.0	3.8	2.2	$\cdots$
	$\Delta\alpha_K$	8.79×10^{-2}	7.65×10^{-2}	4.37×10^{-2}	$\cdots$
Physical Model	$\Delta\Omega_m h^2$	2.12×10^{-3}	2.17×10^{-3}	1.19×10^{-3}	0.79
Arbitrary $K_0(z)$	$\Delta\Omega_{DE}$	3.66×10^{-3}	7.11×10^{-3}	2.56×10^{-3}	0.79
	Δw_0	7.73×10^{-2}	6.05×10^{-2}	2.61×10^{-2}	0.55
	Δw_a	0.23	0.17	9.25×10^{-2}	0.68
	$\Delta\sigma_8$	1.45×10^{-2}	7.85×10^{-3}	3.62×10^{-3}	0.52
	$\Delta\sigma_{XR}$	7.79×10^{-3}	$\cdots$	5.61×10^{-3}	$\cdots$
	$\Delta\sigma_{SZ}$	$\cdots$	9.77×10^{-3}	6.74×10^{-3}	$\cdots$
	Δf_g	2.48×10^{-2}	3.94×10^{-2}	1.23×10^{-2}	$\cdots$
	$< \Delta K_0 >$	2.2	2.8	1.5	$\cdots$